ACS APPLIED NANO MATERIALS

www.acsanm.org Article

Unraveling the Origin of Interfacial Oxidation of InP-Based Quantum Dots: Implications for Bioimaging and Optoelectronics

Ajit Vikram, Arwa Zahid, Saket S. Bhargava, Hyukjin Jang, Andre Sutrisno, Ankur Khare, Peter Trefonas, Moonsub Shim, and Paul J. A. Kenis*

Cite This: *ACS Appl. Nano Mater.* 2020, 3, 12325−12333 Read Online

ACCESS | Metrics & More | Article Recommendations | Supporting Information

ABSTRACT: Indium phosphide core/shell nanocrystals hold promise to replace heavy-metal-based emissive materials for bioimaging and optoelectronic applications. Uniformity of the shell passivation and the interfacial defects are critical for achieving improved optical properties. A combination of Fourier-transform infrared spectroscopy (FTIR) and liquid and solid-state NMR spectroscopy revealed a strong correlation between interfacial oxidation and photoluminescence of InP-based core/shell quantum dots. Using an automated sequential shell growth approach enabled efficient flow synthesis of InP/ZnSe/ZnS quantum dots, exhibiting high-quantum yields and narrow emission line widths. Feeding individual precursors into the reactor channel in a sequential fashion combined with inline reaction monitoring enabled precise control over layer-by-layer shell passivation of the core particles. Our findings suggest that an unintentional aminolytic reaction between oleylamine and carboxylates (two most commonly used starting materials for colloidal synthesis) introduces oxidative defects during the shelling process, thus limiting their optical properties.

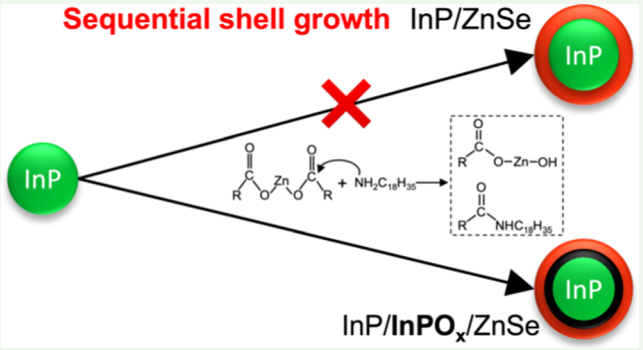

KEYWORDS: *quantum dots, indium phosphide, interfacial oxidation, core/shell nanocrystals, flow synthesis*

INTRODUCTION

Colloidal quantum dots of heavy-metal-free semiconductor materials are of significant interest for applications ranging from bioimaging to optoelectronic applications.[1−3] Among various heavy-metal-free candidates, indium phosphide (InP)-based quantum dots (QDs) have recently emerged as a promising alternative.[4−8] Despite significant advances, the optical properties of InP-based core/shell QDs using the most commonly used batch synthesis approach are limited to typical photoluminescence (PL) quantum yields (QY) in the range of 50−70% and line widths in the range of 50−80 nm.[9−13] Water-induced oxidation of the highly oxyphilic InP surface is considered a major bottleneck for achieving enhanced optical properties. The presence of carboxylic acids in the most widely used InP QD synthesis recipe (using silylphosphines[14,15]) promotes oxidation by the formation of water as a ketonization reaction byproduct.[16,17] More recent studies using the aminophosphine-based synthesis route have yielded oxide-free InP QDs.[18,19] However, despite starting with an oxide-free InP core, the interfacial phosphorous atoms are subsequently oxidized during the shelling of core nanocrystals with ZnSe or ZnS. Prior work by Cossairt et al. showed that even a thoroughly degassed core/shell synthesis approach yielded in InP/Zn(Se,S) with phosphorous oxidation as high as 85%.[20] As expected, such a high extent of interfacial oxidation significantly affects the optical properties of the core/shell QDs. Similar trends have been observed for several other classes of oxyphilic semiconductor nanocrystals such as ZnTe-based nanorods and QDs.[21,22] The impact of phosphorous oxidation on the PL properties, however, remains ambiguous. For instance, Tessier et al. showed that oxide-free core/shell InP-based QDs exhibit significantly lower QY compared to QDs with an oxidized interface.[18] On the contrary, etching of the InP core prior to shell growth has enabled the synthesis of high photoluminescent QDs, primarily attributed to the removal of the oxide layer on the InP surface.[4,23] A systematic study to correlate interfacial oxidation with optical properties is critical to understand its role in achieving high-quality nanocrystals.

Additionally, the majority of the work in the area of colloidal semiconductor nanocrystals has utilized different multipot batch synthesis approaches with limited control over reaction conditions as well as heat and mass transfer, thus limiting both

Received: October 20, 2020
Accepted: November 30, 2020
Published: December 10, 2020

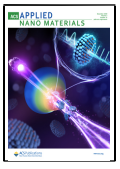

Scheme 1. Schematic Representation of InP/ZnSe/ZnS Core−Shell Synthesis: Precursor Conversion Reaction to Form InP Nuclei and Core Nanocrystals, Followed by Shell Passivation with ZnSe and ZnS Layers[a]

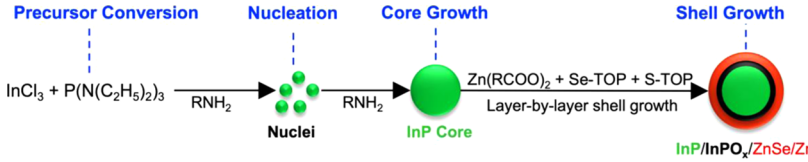

[a]The Core/Shell Nanocrystals Undergo an Unintentional Interfacial Oxidation during the Shell Growth Reaction.

product quality and reproducibility.[24] The use of continuous flow synthesis offers an opportunity to overcome these challenges, which is critical to develop robust manufacturing technologies for the synthesis of QDs.[25−27] Prior studies using flow synthesis for InP-based core/shell QDs resulted in either lower QYs (<40%) or broad PL line width (>60 nm for red emission) despite improved heat and mass transfer.[25,28] Two major reasons that the product quality using flow synthesis approach significantly lags behind their batch counterpart are (1) limited reconfigurability of the process, specifically precursor addition at different points within the reactor, and (2) the inability of adapt most batch synthesis recipe due to use of highly viscous solvents such as high concentration of carboxylate-based precursors for InP synthesis. Flow synthesis of nanocrystals by design is more amenable to scale up by simply scaling the reactor volume while maintaining the same channel diameter. Such scale-up approach will not work for the most batch synthesis of nanocrystals because at higher reaction volume, the nucleation, growth, and precursor mixing conditions will become more sensitive to the heat and mass transfer imitations. In turn, at larger scales, this will lead to a loss of nanocrystal product quality as well as poor process reproducibility. This major advantage of the flow reactor for scalable nanomanufacturing is one of the major motivations for developing chemistries that are more suitable for flow synthesis. The major challenge for nanomanufacturing is to translate the rich chemistry that has been developed in batch syntheses into continuous flow platforms, and very often this translation is not straightforward due to the limited adaptability of batch synthesis conditions. Simultaneous optimization of core nucleation, core growth, and a multiple shelling process is needed for multistep flow synthesis of core/shell nanocrystals with desired optical and structural properties (Scheme 1).

In this work, we elucidate the role of interfacial oxidation on the photoluminescence quantum yield (PLQY) and line width of the InP/ZnSe/ZnS core/shell nanocrystals. A mechanistic study of the core/shell reaction products revealed an unintentional aminolytic reaction as the major source of phosphorous oxidation. The core/shell nanocrystals are synthesized using an automated reconfigurable continuous flow reactor that enables the separation of core nucleation and growth, followed by sequential shelling steps by introducing multiple precursor feeds into the reactor channel. The optimal flow reactor configuration yielded InP/ZnSe/ZnS QDs exhibiting high PLQY and narrow line width.

EXPERIMENTAL SECTION

Chemicals. Indium(III) chloride (99.999%), zinc(II) chloride (>98%), oleylamine (OLAM) (technical grade, 70%), octadecene (ODE) (technical grade, 90%), anhydrous ethanol (<0.005% water), anhydrous hexane (<0.001% water), tris-(diethylamino)phosphine (TDEAP) (97%), selenium powder (100 mesh, 99.99%), trioctylphosphine (TOP) (>97%), zinc stearate (purum, 10−12% Zn basis), and stearic acid were purchased from Sigma-Aldrich. All solvents were degassed and stored inside the glovebox under a nitrogen environment.

Stock Solution Preparation. *Indium Chloride in Oleylamine (0.2 M).* Four millimoles of indium chloride was added to a 50 mL three-neck flask containing 20 mL of degassed oleylamine inside the glovebox. The three-neck flask was then transferred to a Schlenk line for degassing (three cycles of vacuum and nitrogen purge) at 100 °C for 1 h. The stock solution was then kept under positive nitrogen pressure at 60 °C under continuous stirring for flow synthesis experiments.

Zinc Chloride in Oleylamine (1.0 M). Zinc chloride stock solution was also prepared following a similar step as indium chloride stock solution, except 20 mmol of zinc chloride was added to 20 mL of oleylamine inside the glovebox. The stock solution was kept under nitrogen at 60 °C with continuous stirring after degassing. Before starting the flow synthesis experiment, 16 mmol of TDEAP was added to the flask and allowed to mix under continuous stirring.

Zinc Stearate in Octadecene (1.0 M). Twenty millimoles of zinc stearate was added to a 50 mL three-neck flask containing 20 mL of octadecene. For the synthesis of QD1 batch: the mixture was heated until it reached 120 °C and then nitrogen was bubbled through the mixture for 12 h using a needle; for the synthesis of QD2 batch: the mixture was heated under vacuum until it reached 120 °C and then degassed with nitrogen−vacuum cycles for 2 h at 120 °C; for the synthesis of QD4 batch: the mixture was heated at 120 °C for 2 h without the degassing step; for the synthesis of QD3 batch: 2 mmol of stearic acid was added to the zinc stearate and ODE mixture, followed by similar treatment as outlined for QD2 batch. The zinc stearate-containing flask was then kept under nitrogen at 120 °C with continuous stirring.

TOP-Se (1.0 M) and TOP-S (1.0 M). TOP-Se and TOP-S stock solutions were separately prepared by sonicating, 20 mmol of Se or 20 mmol of S in 20 mL of TOP until a clear and well-dissolved solution was obtained.

Flow Synthesis of InP/ZnSe/ZnS QDs. Typically, 0.2 M indium chloride and 1 M zinc chloride (with phosphorous precursor) are pumped through an inline mixer (maintained at 60 °C), followed by a nucleation (at 200 °C) and core growth (160 °C) reactor for the synthesis of InP QDs. In the subsequent reactor stages (four stages in series), 1 M Se, Zn, S, and Zn stock solutions are pumped to the reaction channel in a sequential fashion for the ZnSe/ZnS shell growth reaction. The reactor temperature for shell growth stage is steadily increased across the reactor from 240 to 300 °C with a step increase of 20 °C at each stage. At each stage of the reaction, the reaction mixture is sampled using a sampling valve and characterized using an inline UV−vis and PL flow cell. The reaction products at different stages are collected for ex situ characterization [transmission electron microscopy (TEM), Fourier-transform infrared spectroscopy (FTIR), ^{1}H NMR, and ^{31}P NMR]. The details of the postsynthesis treatment and characterizations are included in the Supporting Information. All process parameters including precursor flow rates, addition of precursors for shell growth, reaction sampling, inline characterization, and data analysis are controlled in an automated fashion using a Matlab script. The details regarding the reactor configuration, design, sampling, and process parameters are outlined in the Supporting Information.

https://dx.doi.org/10.1021/acsanm.0c02814
ACS Appl. Nano Mater. 2020, 3, 12325−12333

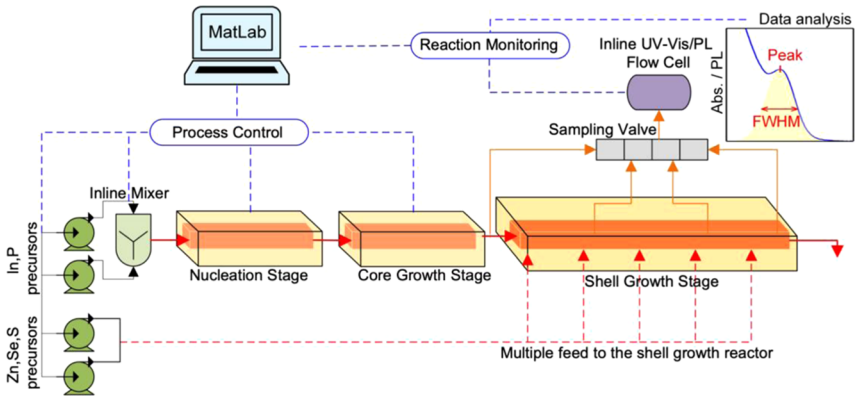

Figure 1. Schematic representation of the reconfigurable automated flow reactor platform showing the three key stages: core nucleation, core growth, and sequential shell growth using multiple feeds along the reactor channel. A sampling valve and an inline UV−vis and PL flow cell are used to monitor products at different stages in the reactor. The process parameters (temperature and flow rate of different stages) and data analysis of the spectra are automated using MatLab.

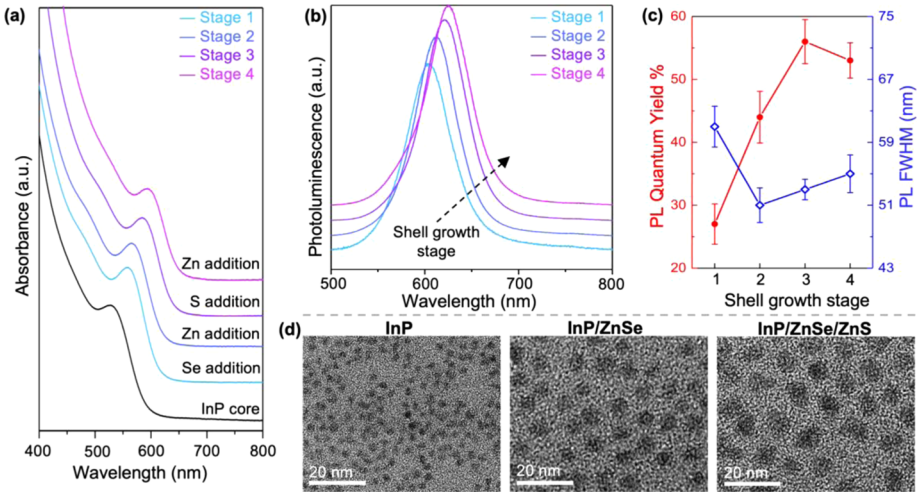

Figure 2. Characterization data of InP/ZnSe/ZnS QD synthesized using an optimized reactor configuration. (a) Absorbance spectra of InP core particles and ZnSe/ZnS shell growth at different stages upon sequential feeding of Se (stage 1), Zn (stage 2), S (stage 3), and Zn (stage 4) to the shell reactor. (b) Normalized photoluminescence spectra and (c) PL quantum yield and FWHM of shelled quantum dots at different stages of the shell reactor. (d) TEM images showing nearly monodisperse core InP (average diameter: 2.7 nm), InP/ZnSe (shell thickness: 1.4 nm), and InP/ZnSe/ZnS (ZnS shell thickness: 0.6 nm).

RESULTS AND DISCUSSION

Prior to discussing the role of interfacial oxidation on the optical properties (PLQY and line width) of core/shell InP-based quantum dots, and the source of in situ oxidation, we first elucidate on the automated flow reactor platform that enabled the synthesis of uniform core/shell InP/ZnSe/ZnS nanocrystals.

Flow Synthesis of InP QDs. To date, several indium and phosphorous precursors for the batch synthesis of InP QDs have been reported in the literature.[9,16,29−31] Among different InP chemistries, silylphosphine and indium carboxylate-based precursors are the most commonly used precursors. However, the high viscosity of indium carboxylates at high concentrations and the high reactivity of the silylphosphines are the major bottleneck for adapting the silylphosphine-based chemistry for the flow synthesis of high-quality InP-based quantum dots.[25] The recent development of aminophoshine-based phosphorous precursors and indium halides-based indium precursors are ideally suited for flow synthesis due to the low viscosity of the reaction mixtures.[9,19,32] The lower reactivity and nonpyrophoric properties of aminophosphine precursors enable an economical and easy-to-implement synthesis of InP QDs using flow reactors. Recently, Owen et al. reported that modifying tris(dimethyl)aminophosphine to other alkyl-based derivatives can significantly shift the nucleation-growth kinetics to be limited by precursor conversion reaction.[33] The substituted derivatives of amino-phosphine precursors' results in significantly different growth kinetics pathway compared to the tris-aminophosphine-based phosphorous precursors. Alternatively, the nucleation-growth kinetics of InP using tris(diethyl)aminophosphine precursors can also be tuned by spatial separation of nucleation and growth using a multistage flow reactor configuration.[34]

Automated Sequential Shell Growth Flow Reactor. Figure 1 shows the schematic of the automated modular flow reactor platform, consisting of three primary components: (i) automated control of process parameters such as precursor flow rates, reactor temperature, and precursor concentration; (ii) automated product sampling and analysis using inline UV−vis and PL spectroscopy; and (iii) sequential addition of multiple precursor streams along the shell growth reactor channel. The reactor modules comprise a core nucleation

https://dx.doi.org/10.1021/acsanm.0c02814
ACS Appl. Nano Mater. 2020, 3, 12325−12333

reactor, a core (InP) growth reactor, and a multistage shell (ZnSe/ZnS) growth reactor. Custom-designed SMX static mixers[35] are housed within the reactor channels for rapid mixing of the feed streams with the reactant stream.[25] A detailed description of the reactor platform is included in the Supporting Information (Figure S1).

Utilizing the aforementioned flow synthesis platform, we synthesized InP/ZnSe/ZnS nanocrystals by first synthesizing the InP core nanocrystals in the first two stages: (i) nucleation at high temperature (200 °C) and small residence time (5 s) and (ii) subsequent InP growth at a lower temperature (160 °C) for 20 min. The synthesis conditions: nucleation at a higher temperature and short residence time and growth at a lower temperature for longer residence time is based on the hypothesis that at a higher temperature, the burst of nuclei is initiated in the reaction for a small reaction time (5 s), followed by growth at a significantly lower temperature, which would prevent the formation of any additional nuclei and enable spatial separation of nucleation and growth process. The precise conditions for the core nucleation and growth conditions, however, do not represent a statistically optimized condition. The spatial separation of nucleation and growth, induced by process parameters, is unique to the flow reactor configuration and is not feasible in most commonly used hot-injection-based batch syntheses as has been previously demonstrated for PbS and CdSe QDs.[34,36] Future work using similar spatially separated nucleation and growth flow reactors can allow further improvement and optimization of the reaction condition. The first absorption maximum of the synthesized InP nanocrystals using the abovementioned process parameters appeared at 525 nm (Figure 2a), with an average core diameter of 2.7 nm (Figure 2d) and absorbance full width at half maximum (FWHM) of 51 nm, suggesting high monodispersity in size. In the subsequent stages, shell precursor streams are mixed in the reactant stream consisting of InP nanocrystals for shell growth. The ability to continuously monitor the reaction progress using inline UV−vis and PL measurements enabled the optimization of the shelling process by reconfiguring the volume of the individual shell growth stages, achieved by adjusting the position where shell precursors are introduced. We hypothesize that a layer-by-layer uniform shell passivation of core nanocrystals in flow will yield InP/ZnSe/ZnS quantum dots with high PLQY and narrow PL line width. By leveraging the inline UV−vis/PL spectral monitoring of the reaction with the reconfigurable flow reactor platform, an optimal four-stage shell growth strategy was achieved: Se precursor fed to stage 1 (240 °C), Zn precursor fed to stage 2 (260 °C), S precursor fed to stage 3 (280 °C), and Zn precursor fed to stage 4 (300 °C). Previously reported shell growth processes using flow reactor configuration are largely limited by the reconfigurability of the process. Specifically, all shell precursors are mixed and added for shell growth in a single-stage reactor.[25,28] However, the high concentration of shell precursors in the reaction mixture prevents uniform shell growth around the core nanocrystals. Sequential addition of shell precursors in batch syntheses has enabled a layer-by-layer growth strategy, yielding core/shell nanocrystals with very high optical quality.[9] The reconfigurability of the flow reactor platform presented in this work allows sequential addition of shell precursors in flow channels to maintain a low-shell precursor concentration throughout the shelling process, thus enabling a uniform layer-by-layer shell growth. Apart from the sequential addition of the shell precursors, the shell growth temperature is increased steadily across different stages from 240 to 300 °C to compensate for the increased surface area of the shelled nanocrystals as the shelling reaction progresses. Higher reaction temperatures at a later stage of the shelling process enable increased shell growth rate and thus maintain lower residence time for the shell growth stage. The schematic of the optimal six-stage configuration of the flow reactor platform and reaction conditions is shown in Figure S3. The passivation of core InP with the ZnSe/ZnS shell is accompanied with an incremental red shift in the peak position of the UV−vis spectra of the product stream after each shell growth stage (Figure 2a). The UV−vis and PL spectra correspond to the reaction mixture sampled at different reactor stages. As the shell thickness increases along the shell growth reaction stages, the emission peak position shows a significant red shift from 593 nm after stage 1 to 623 nm after stage 4 (Figure 2b). The shift in the PL peak position is accompanied with a steady increase in PLQY from 27% at the beginning of the shelling stage to a maximum of 56% after stage 3 (Figure 2c). The initial increase in PL of the reaction mixture sampled from stage 1 corresponds to the ZnSe shell growth, which is initiated in stage 1 upon reaction between excess zinc precursor present in the core reaction mixture and Se precursors added to the reactor channel. Additionally, the red-emitting ZnSe/ZnS passivated QDs exhibit a narrow PL line width (FWHM ∼ 50−55 nm), a significant advancement compared to prior work in the flow synthesis of emissive InP-based nanocrystals.[25,28] The enhanced PLQY and narrow line width achieved with the reconfigurable flow reactor platform further highlight the critical role of the precisely controlled sequential shell growth strategy for achieving the enhanced optical properties of core/shell quantum dots.

Correlation between Interfacial Oxidation and Photoluminescence. Despite extensive synthesis optimization of InP-based core/shell QDs, the majority of prior work reports PL line widths in the range of 50−70 nm and PLQY in the range of 50−70% for red-emitting QDs.[9,11,37,38] Although these reports are based on conventional batch synthesis strategies, our approach of using an optimal flow reactor configuration for shell growth also yielded InP-based QDs with PL line widths >50 nm and QYs < 60%. The extent of interfacial oxidative defects is regarded as one of the most critical factors limiting the optical properties of InP-based QDs.

To understand the impact of the oxidized interface on the optical properties of the shelled QDs, we performed a systematic study by synthesizing QDs spanning a range of phosphorous oxidation levels. Four different batches of InP/ZnSe/ZnS QDs were synthesized (labeled as QD1, QD2, QD3, QD4). All synthesis conditions, reactor configuration, and process parameters were kept identical (including InP core synthesis conditions, shell growth stage temperatures, shell precursor concentrations), except the treatment of shell precursor prior to the synthesis: (i) bubbling under nitrogen overnight (QD1), (ii) standard degassing for 2 h (QD2), (iii) addition of a small amount of (10% by mole) stearic acid (QD3), and (iv) preparing precursors without degassing (QD4). The synthesis conditions and precursor preparation methods for all of these samples (QD1−4) are outlined in the Experimental Section (see the Supporting Information). All QD samples used for ex situ characterization and analysis (NMR and FTIR) are synthesized using the abovementioned

https://dx.doi.org/10.1021/acsanm.0c02814
ACS Appl. Nano Mater. 2020, 3, 12325−12333

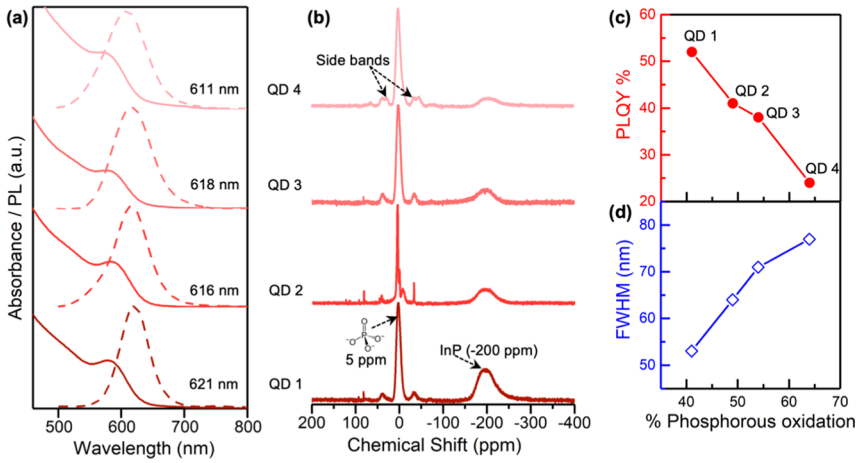

Figure 3. (a) UV−vis and PL spectra of different batches of InP/ZnSe/ZnS QDs: QD1, QD2, QD3, and QD4. (b) ^{31}P MAS SSNMR spectra of the shelled QD batches showing different extents of oxidation. The resonance spectra corresponding to crystalline InP (−200 ppm) and to oxidized phosphorous (5 ppm) are labeled. The effect of (c) PLQY and (d) emission FWHM as a function of % phosphorous oxidation at the core/shell interface.

automated flow reactor platform. The shelled QDs, starting with identical InP core, each exhibited a PL emission peak in the range of 611−621 nm, suggesting that the core size and the shell thickness of these QDs remain very similar (Figure 3a). However, the PL line widths and QYs of these batches varied significantly from one another in the range of 50−80 nm and 21−53%, respectively. As shown in the prior works, solid-state NMR (SSNMR) allows for quantitative estimation of InP-oxidation as it can distinguish between the unoxidized InP and oxidized $InPO_x$ present on the core−shell interface.[19] The separate resonance peaks for unoxidized and oxidized phosphorous allow quantification of the extent of interfacial oxidation of InP-based core/shell quantum dots by evaluating the area under the curve for the resonance peaks observed in the SSNMR. Figure 3b shows the magic angle spinning (MAS) ^{31}P NMR spectra of InP/ZnSe/ZnS powder, obtained for the different batches (QD1−4). Samples for SSNMR analysis were obtained through an oxygen-free purification, drying, and packing procedure inside a nitrogen-filled glovebox (see the Experimental Section in the Supporting Information). As shown in Figure 3b, the single resonance at −200 ppm corresponds to the unoxidized phosphorous in the core/shell QDs. Additionally, the large peak at ∼5 ppm corresponds to the oxidized phosphorous species ($InPO_x$). Moreover, no residual oxidation is observed in the spectra corresponding to the InP core only samples (Figure S4), consistent with our prior work. The oxide-free InP core surface is attributed to the use of aminophosphine-based chemistry for the synthesis of core nanocrystals. However, during the shelling process, a significant amount of interfacial phosphorous is oxidized. The effective bubbling of the shell precursor solutions with nitrogen prior to commencing synthesis minimizes interfacial oxidation (QD1, 41%).[23] Similarly, a significantly higher oxidation of up to 64% is observed when the shell precursor solutions are prepared without the vacuum degassing step prior to synthesis (QD4). Additionally, the emission peak positions of the shelled QDs also remain similar (all within the range of 611−621 nm, Figure 3a), suggesting a similar shell thickness for all samples, despite different treatment of the shell precursor solutions prior to shelling. The shelled QD samples (QD1−4) are thus well suited for a comparative study regarding the effect of interfacial phosphorous oxidation on PL properties. Since the core sizes and shell thicknesses of the synthesized QD samples remain identical, and the reaction conditions, ligands, and solvents for the synthesis are similar, any effect on the PL properties can be attributed directly to the extent of phosphorous oxidation at the core/shell interface. As shown in Figure 3c, an observed increase in oxidation at the core/shell interface correlates linearly with a decrease in PLQY and an increase in PL line width (FWHM). Previously, Tessier et al. reported that oxide-free InP-based QDs exhibit a lower PLQY compared to equivalent oxidized InP-based QDs.[18] The suppressed emission intensity was hypothesized to be a direct result of the absence of a phosphate interface in these core/shell nanocrystals. In contrast, here we observe a drastically different trend: core/shell QDs with a lower interfacial oxidation exhibit higher PLQYs and narrower line widths. A possible explanation for the different trends observed by Teisser et al. could be their use of different precursors (zinc halides for oxide-free QDs and long-chain carboxylates for oxidized QDs), which are not well suited for a direct comparative study regarding the role of interfacial oxidation. Alternatively, this different trend in the role of oxidation on PL properties, reported by Tessier et al., can also be due to the difference in the extent of oxidation in the core/shell samples analyzed in their work (two clusters: <3 and 55−60% oxidation). It is indeed possible that the trend of improved PL properties with decreasing interfacial oxidation shifts as it approaches a nearly nonoxidized interface that yields in very low PLQY. Our observations also explain some of the more recent reports of oxide-free synthesis of InP-based QDs, showing that efficient HF etching of the oxide layer prior to the shelling process is critical to achieve QDs exhibiting near-unity QYs.[4] The addition of HF along with the injection of shell precursors is hypothesized to be critical for preventing reoxidation of the InP surface during shell growth, which is induced due to an unintentional decarboxylative coupling reaction of fatty acids.

Origin of Interfacial Oxidation. Due to the presence of oxyphilic phosphorous in InP-based QDs, most commonly reported synthesis approaches have yielded InP/ZnSe(S) nanocrystals with interfacial oxidation in the range of 50−85%, depending on the starting precursors used in the synthesis.[20] Prior work hypothesized the source of phospho-

https://dx.doi.org/10.1021/acsanm.0c02814
ACS Appl. Nano Mater. 2020, 3, 12325−12333

rous oxidation to be an outcome of an unintentional decarboxylative coupling reaction of excess carboxylic acid present during core and shell growth, yielding the equivalent ketone, carbon dioxide, and water as side products.[17] The primary source of the excess acid in the reaction mixture is attributed to the use of carboxylic acids for the preparation of zinc or indium precursors prior to the synthesis. However, the oxidized InP interface has also been observed for samples prepared in the absence of excess free carboxylic acid. We observe similar oxidation during the shelling of unoxidized InP core with zinc carboxylate salts (Figure 3). The origin of these high extents of oxidation of InP cores in the absence of carboxylic acid and water impurities in the reaction mixture thus remains ambiguous.

To further rationalize the source of unintentional oxidation during shell growth, we characterized the crude QD products using attenuated total reflectance (ATR)-Fourier-transform infrared spectroscopy (FTIR). No major carbonyl stretching peaks are present in the region of 1700−1780 cm^{-1} of ATR-FTIR spectra of the crude QD products collected from different shelled QD samples (QD1−4; Figure 4a). The presence of any alkyl anhydride, ketone, or carboxylic acid would exhibit IR peak between 1700 and 1780 cm^{-1}.[39] This confirms the absence of both free acids and any anhydride or ketone that may form due to the decarboxylative coupling reactions of free acids. Based on the prior literature on different

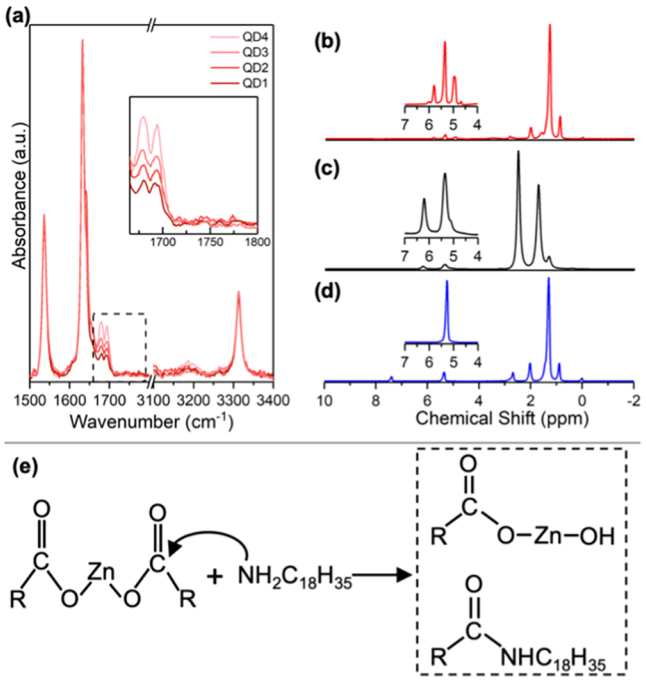

Figure 4. (a) ATR-FTIR spectra of different batches of InP/ZnSe/ZnS QDs: QD1, QD2, QD3, and QD4. The inset shows the scaled spectral region between 1660 and 1800 cm^{-1}. ^{1}H NMR spectra of (b) synthesized InP/ZnSe/ZnS (QD1), (c) zinc stearate precursor solution used for shell growth, and (d) InP core only crude solution. The inset in (b)−(d) shows the NMR spectra, scaled in the region of interest 4−7 ppm. (e) Schematic representation of the proposed source of interfacial oxidation: aminolytic reaction between zinc stearate salt and oleylamine yields an amide and a hydroxide-containing species, which induces phosphorous oxidation. The structure of species shown in the reaction is simplified representation of the molecule.

functional groups, the IR peaks in the region of 1500−3400 cm^{-1} are assigned. The major peaks at 1538, 1642, and 3310 cm^{-1} are attributed to, respectively, the asymmetric C−O "bond and a half" stretching from the carboxylate salt, C═C stretching from the octadecene solvent, and N−H stretching from oleylamine.[40−42] Additionally, two strong and unexpected peaks at 1680 and 1694 cm^{-1} are assigned to carbonyl stretching due to the presence of secondary amides in the crude shelled QD solution.[43] Based on prior reports, a possible route to the formation of these amide byproducts can be the amidation reaction between free carboxylic acids and oleylamine, thus yielding water as an additional oxidizing product.[44] The amide formation is expected due to the presence of excess carboxylic acids present in the reaction mixture. However, the absence of any carbonyl stretching peaks from free acid in the region of 1700−1780 cm^{-1} in the FTIR spectra of shell precursors (Figure S5) and the crude solution of shelled QDs eliminate the possibility of amidation between oleylamine and carboxylic acid to be the key source of phosphorous oxidation during the shelling process. Additional control experiments using ^{1}H NMR spectral analysis of the crude InP core product (Figure 4d), shell precursors (Figure 4c) and the crude solution of shelled QDs (Figure 4b) also confirmed the absence of peaks arising from carboxylic acid protons (no strong resonance with a chemical shift in the region of 8−10 ppm). The NMR spectrum of the shelled QD solution exhibits a new, strong resonance peak (absent in both core product and shell precursors NMR spectra) with a chemical shift of 5.8 ppm, typical of protons from an amide product (O═C-N**H**R). The neighboring peak with a chemical shift of 5.3 ppm is assigned to the protons from the C═C bonds in oleylamine and octadecene. The presence of resonance peaks of the amide proton in the shelled QD product further confirms our conclusions based on FTIR spectral analysis.

Based on the evidence obtained from FTIR and NMR, we propose that an aminolytic reaction of zinc stearate salt (from shell precursors) with oleylamine (solvent and ligand for InP core synthesis) forms oleyl stearamide and a−O−Zn−OH intermediate (Figure 4e). Thus, the unintentional formation of this hydroxide species during the shelling process is attributed to be the primary source of oxidation. The hydroxide intermediate species (−O−Zn−O−H) can further react to form zinc oxide and water molecules during the shelling process at elevated temperatures. Prior reports have attributed the ketonization or amidation reaction of carboxylic acids as the primary source of phosphorous oxidation.[18,20,44,45] Our findings suggest that even in the absence of free acids, significant interfacial oxidation at core/shell interface is observed, primarily induced by an aminolytic reaction between carboxylate salt and oleylamine. It is indeed possible that despite the absence of free carboxylic acids, stearate salts in equilibrium with oleylamine can form a stearate−oleylammonium pair, which can then react at high reaction temperatures to yield an amide and a hydroxide species, which is primarily responsible for the oxidation of InP during the shell growth. The strong correlation between the interfacial oxidation and optical properties further implies that future studies for synthesizing QDs exhibiting high PLQY should focus on identifying alternate synthesis recipes. Avoiding aminolytic side reaction would require InP core synthesis recipes that do not require primary amine as solvent or ligand. However, primary amine is also required for the InP precursor conversion reaction in which aminophosphine precursors undergo a 3-fold

https://dx.doi.org/10.1021/acsanm.0c02814
ACS Appl. Nano Mater. 2020, 3, 12325−12333

transamination to form InP monomers for nucleation and growth.[19,37] Identifying InP-based chemistry that is free of primary amines and carboxylates thus remains challenging but critical to develop a robust and HF-free synthesis strategy for manufacturing of high-quality InP-based core/shell QDs. Similar aminolytic reactions at elevated reaction temperatures have also been reported as efficient routes for the synthesis of metal oxide nanostructures[46] and indium oxide shell around the InP core nanocrystals.[47] Our findings also explain the high extent of surface oxidation observed in other classes of semiconductor nanocrystals, such as ZnTe and ZnTe/ZnSe QDs in which primary amines and carboxylate salts are abundantly present during synthesis at elevated temperature.[21,22]

CONCLUSIONS

In summary, we demonstrated a systematic investigation into the interfacial oxidation of the core/shell quantum dots using SSNMR revealed a linearly declining trend in the optical properties (PLQYs and line widths) of InP-based core/shell quantum dots with an increase in the extent of interfacial oxidation, in contrast to hypotheses reported previously. The high extent of interfacial oxidation (>40% phosphorous) thus limits the synthesis of core/shell QDs exhibiting higher PLQYs. Additional study of the reaction products using ATR-FTIR and ^{1}H NMR spectroscopy revealed that even in the absence of free carboxylic acids, an aminolytic reaction between oleylamine and carboxylate salts acts as the primary source of hydroxide intermediate species, responsible for the oxidation of the oxide-free InP core during the shelling process. The aminolytic reaction pathway proposed in this work also addresses the high extent of oxidation observed in several other heavy-metal-free quantum dots such as ZnTe/ZnSe, a major bottleneck for achieving high PLQYs for Cd-free QDs.

The synthesis of InP/ZnSe/ZnS QDs that exhibit narrow photoluminescence line widths (∼50 nm) and high-quantum yields (>50%) is enabled by an automated reconfigurable continuous flow reactor platform. Future work will focus on identifying statistically optimized reaction conditions for core growth (separation of nucleation and growth in flow) and shell growth (sequential addition of precursors in flow) reactions to further improve the photoluminescent properties of InP-based quantum dots. Notably, the reconfigurability of the platform, integrated with inline product monitoring, allows for sequential growth of shell materials on core nanocrystals in an efficient and reproducible fashion, a significant advance in continuous flow layer-by-layer growth of nanocrystals.

The insights learned from this work pave the way for future studies in the area of synthesis of oxyphilic nanocrystals well beyond InP-based core/shell materials, which should focus on identifying alternate synthesis recipes that avoid the presence of an amine-carboxylate pair, thus preventing surface and interfacial oxidation. Furthermore, oxide-free interfaces are critical to achieve enhanced optoelectronic properties of heavy-metal-free semiconductor nanocrystals for applications ranging from bioimaging, solar cells, and display technologies.

ASSOCIATED CONTENT

Supporting Information

The Supporting Information is available free of charge at https://pubs.acs.org/doi/10.1021/acsanm.0c02814.

Experimental procedures, synthesis protocol, and details of the continuous flow platform are included; additional NMR and FTIR spectra of other samples are related to the synthesis (PDF)

AUTHOR INFORMATION

Corresponding Author

Paul J. A. Kenis − *Department of Chemical and Biomolecular Engineering, University of Illinois at Urbana-Champaign, Urbana, Illinois 61801, United States;* orcid.org/0000-0001-7348-0381; Email: kenis@illinois.edu

Authors

Ajit Vikram − *Department of Chemical and Biomolecular Engineering, University of Illinois at Urbana-Champaign, Urbana, Illinois 61801, United States;* orcid.org/0000-0002-7397-3431

Arwa Zahid − *Department of Chemical and Biomolecular Engineering, University of Illinois at Urbana-Champaign, Urbana, Illinois 61801, United States*

Saket S. Bhargava − *Department of Chemical and Biomolecular Engineering, University of Illinois at Urbana-Champaign, Urbana, Illinois 61801, United States*

Hyukjin Jang − *Department of Bioengineering, University of Illinois at Urbana-Champaign, Urbana, Illinois 61801, United States*

Andre Sutrisno − *NMR/EPR Laboratory, School of Chemical Sciences, University of Illinois at Urbana-Champaign, Urbana, Illinois 61801, United States;* orcid.org/0000-0003-2308-5708

Ankur Khare − *DuPont Electronics & Imaging, Marlborough, Massachusetts 01752, United States*

Peter Trefonas − *DuPont Electronics & Imaging, Marlborough, Massachusetts 01752, United States*

Moonsub Shim − *Department of Materials Science and Engineering, University of Illinois at Urbana-Champaign, Urbana, Illinois 61801, United States;* orcid.org/0000-0001-7781-1029

Complete contact information is available at: https://pubs.acs.org/10.1021/acsanm.0c02814

Notes

The authors declare no competing financial interest.

ACKNOWLEDGMENTS

TEM imaging was carried out in the Frederick Seitz Materials Research Laboratory Central Research Facilities, University of Illinois. NMR spectroscopy was performed at the School of Chemical Sciences NMR Lab. We gratefully acknowledge financial support from DuPont Electronics & Imaging (research agreement #226772AC) and National Science Foundation (research grant #1825356).

REFERENCES

(1) Martynenko, I. V.; Litvin, A. P.; Purcell-Milton, F.; Baranov, A. V.; Fedorov, A. V.; Gun'ko, Y. K. Application of Semiconductor Quantum Dots in Bioimaging and Biosensing. *J. Mater. Chem. B* **2017**, *5*, 6701−6727.

(2) Kagan, C. R.; Lifshitz, E.; Sargent, E. H.; Talapin, D. V. Building devices from colloidal quantum dots. *Science* **2016**, *353*, No. aac5523.

(3) Shivaji, K.; Mani, S.; Ponmurugan, P.; De Castro, C. S.; Davies, M. L.; Balasubramanian, M. G.; Pitchaimuthu, S. Green-Synthesis-Derived CdS Quantum Dots Using Tea Leaf Extract: Antimicrobial,

Bioimaging, and Therapeutic Applications in Lung Cancer Cells. *ACS Appl. Nano Mater.* **2018**, *1*, 1683−1693.
(4) Won, Y. H.; Cho, O.; Kim, T.; Chung, D. Y.; Kim, T.; Chung, H.; Jang, H.; Lee, J.; Kim, D.; Jang, E. Highly Efficient and Stable InP/ZnSe/ZnS Quantum Dot Light-Emitting Diodes. *Nature* **2019**, *575*, 634−638.
(5) Mushonga, P.; Onani, M. O.; Madiehe, A. M.; Meyer, M. Indium Phosphide-Based Semiconductor Nanocrystals and Their Applications. *J. Nanomater.* **2012**, *2012*, No. 869284.
(6) Thomas, A.; Nair, P. V.; Thomas, K. G. InP Quantum Dots: An Environmentally Friendly Material with Resonance Energy Transfer Requisites. *J. Phys. Chem. C* **2014**, *118*, 3838−3845.
(7) Cossairt, B. M. Shining Light on Indium Phosphide Quantum Dots: Understanding the Interplay among Precursor Conversion, Nucleation, and Growth. *Chem. Mater.* **2016**, *28*, 7181−7189.
(8) Derfus, A. M.; Chan, W. C. W.; Bhatia, S. N. Probing the Cytotoxicity of Semiconductor Quantum Dots. *Nano Lett.* **2004**, *4*, 11−18.
(9) Tessier, M. D.; Dupont, D.; De Nolf, K.; De Roo, J.; Hens, Z. Economic and Size-Tunable Synthesis of InP/ZnE (E = S, Se) Colloidal Quantum Dots. *Chem. Mater.* **2015**, *27*, 4893−4898.
(10) Kim, K.; Yoo, D.; Choi, H.; Tamang, S.; Ko, J. H.; Kim, S.; Kim, Y. H.; Jeong, S. Halide-Amine Co-Passivated Indium Phosphide Colloidal Quantum Dots in Tetrahedral Shape. *Angew. Chem., Int. Ed.* **2016**, *55*, 3714−3718.
(11) Dupont, D.; Tessier, M. D.; Smet, P. F.; Hens, Z. Indium Phosphide-Based Quantum Dots with Shell-Enhanced Absorption for Luminescent Down-Conversion. *Adv. Mater.* **2017**, *29*, No. 1700686.
(12) Reid, K. R.; McBride, J. R.; Freymeyer, N. J.; Thal, L. B.; Rosenthal, S. J. Chemical Structure, Ensemble and Single-Particle Spectroscopy of Thick-Shell InP-ZnSe Quantum Dots. *Nano Lett.* **2018**, *18*, 709−716.
(13) Clarke, M. T.; Viscomi, F. N.; Chamberlaing, T. W.; Hondow, N.; Adawi, A. M.; Sturge, J.; Erwin, S. C.; Bouillarde, J. S. G.; Tamang, S.; Stasiuk, G. J. Synthesis of Super Bright Indium Phosphide Colloidal Quantum Dots through Thermal Diffusion. *Commun. Chem.* **2019**, *2*, 1−7.
(14) Gary, D. C.; Glassy, B. A.; Cossairt, B. M. Investigation of Indium Phosphide Quantum Dot Nucleation and Growth Utilizing Triarylsilylphosphine Precursors. *Chem. Mater.* **2014**, *26*, 1734−1744.
(15) Allen, P. M.; Walker, B. J.; Bawendi, M. G. Mechanistic Insights into the Formation of InP Quantum Dots. *Angew. Chem., Int. Ed.* **2010**, *49*, 760−762.
(16) Tamang, S.; Lincheneau, C.; Hermans, Y.; Jeong, S.; Reiss, P. Chemistry of InP Nanocrystal Syntheses. *Chem. Mater.* **2016**, *28*, 2491−2506.
(17) Cros-Gagneux, A.; Delpech, F.; Nayral, C.; Cornejo, A.; Coppel, Y.; Chaudret, B. Surface Chemistry of InP Quantum Dots: A Comprehensive Study. *J. Am. Chem. Soc.* **2010**, *132*, 18147−18157.
(18) Tessier, M. D.; Baquero, E. A.; Dupont, D.; Grigel, V.; Bladt, E.; Bals, S.; Coppel, Y.; Hens, Z.; Nayral, C.; Delpech, F. Interfacial Oxidation and Photoluminescence of InP-Based Core/Shell Quantum Dots. *Chem. Mater.* **2018**, *30*, 6877−6883.
(19) Vikram, A.; Zahid, A.; Bhargava, S. S.; Keating, L. P.; Sutrisno, A.; Khare, A.; Trefonas, P.; Shim, M.; Kenis, P. J. A. Mechanistic Insights into Size-Focused Growth of Indium Phosphide Nanocrystals in the Presence of Trace Water. *Chem. Mater.* **2020**, *32*, 3577−3584.
(20) Stein, J. L.; Holden, W. M.; Venkatesh, A.; Mundy, M. E.; Rossini, A. J.; Seidler, G. T.; Cossairt, B. M. Probing Surface Defects of InP Quantum Dots Using Phosphorus K alpha and K beta X-ray Emission Spectroscopy. *Chem. Mater.* **2018**, *30*, 6377−6388.
(21) Lincheneau, C.; Amelia, M.; Oszajca, M.; Boccia, A.; D'Orazi, F.; Madrigale, M.; Zanoni, R.; Mazzaro, R.; Ortolani, L.; Morandi, V.; Silvi, S.; Szacilowski, K.; Credi, A. Synthesis and Properties of ZnTe and ZnTe/ZnS Core/Shell Semiconductor Nanocrystals. *J Mater Chem C* **2014**, *2*, 2877−2886.
(22) Ji, B. T.; Panfil, Y. E.; Banin, U. Heavy-Metal-Free Fluorescent ZnTe/ZnSe Nanodumbbells. *ACS Nano* **2017**, *11*, 7312−7320.
(23) Li, Y.; Hou, X. Q.; Dai, X. L.; Yao, Z. L.; Lv, L. L.; Jin, Y. Z.; Peng, X. G. Stoichiometry-Controlled InP-Based Quantum Dots: Synthesis, Photoluminescence, and Electroluminescence. *J. Am. Chem. Soc.* **2019**, *141*, 6448−6452.
(24) Pu, Y.; Cai, F. H.; Wang, D.; Wang, J. X.; Chen, J. F. Colloidal Synthesis of Semiconductor Quantum Dots toward Large Scale Production: A Review. *Ind. Eng. Chem. Res.* **2018**, *57*, 1790−1802.
(25) Vikram, A.; Kumar, V.; Ramesh, U.; Balakrishnan, K.; Oh, N.; Deshpande, K.; Ewers, T.; Trefonas, P.; Shim, M.; Kenis, P. J. A.; Millifluidic, A. Reactor System for Multistep Continuous Synthesis of InP/ZnSeS Nanoparticles. *ChemNanoMat* **2018**, *4*, 943−953.
(26) Abdel-Latif, K.; Epps, R. W.; Kerr, C. B.; Papa, C. M.; Castellano, F. N.; Abolhasani, M. Facile Room-Temperature Anion Exchange Reactions of Inorganic Perovskite Quantum Dots Enabled by a Modular Microfluidic Platform. *Adv. Funct. Mater.* **2019**, *29*, No. 1900712.
(27) Skrabalak, S. E.; Brutchey, R. L. Going with the Flow: Continuous Flow Routes to Colloidal Nanoparticles. *Chem. Mater.* **2016**, *28*, 1003−1005.
(28) Baek, J.; Shen, Y.; Lignos, I.; Bawendi, M. G.; Jensen, K. F. Multistage Microfluidic Platform for the Continuous Synthesis of III-V Core/Shell Quantum Dots. *Angew. Chem., Int. Ed.* **2018**, *57*, 10915−10918.
(29) Li, L.; Protiere, M.; Reiss, P. Economic synthesis of high quality InP nanocrystals using calcium phosphide as the phosphorus precursor. *Chem. Mater.* **2008**, *20*, 2621−2623.
(30) Harris, D. K.; Bawendi, M. G. Improved Precursor Chemistry for the Synthesis of III-V Quantum Dots. *J. Am. Chem. Soc.* **2012**, *134*, 20211−20213.
(31) Gary, D. C.; Terban, M. W.; Billinge, S. J. L.; Cossairt, B. M. Two-Step Nucleation and Growth of InP Quantum Dots via Magic-Sized Cluster Intermediates. *Chem. Mater.* **2015**, *27*, 1432−1441.
(32) Buffard, A.; Dreyfuss, S.; Nadal, B.; Heuclin, H.; Xu, X. Z.; Patriarche, G.; Mezailles, N.; Dubertret, B. Mechanistic Insight and Optimization of InP Nanocrystals Synthesized with Aminophosphines. *Chem. Mater.* **2016**, *28*, 5925−5934.
(33) McMurtry, B. M.; Qan, K.; Teglasi, J. K.; Swarnakar, A. K.; De Roo, J.; Owen, J. S. Continuous Nucleation and Size Dependent Growth Kinetics of Indium Phosphide Nanocrystals. *Chem. Mater.* **2020**, *32*, 4358−4368.
(34) Pan, J.; El-Ballouli, A. O.; Rollny, L.; Voznyy, O.; Burlakov, V. M.; Goriely, A.; Sargent, E. H.; Bakr, O. M. Automated Synthesis of Photovoltaic-Quality Colloidal Quantum Dots Using Separate Nucleation and Growth Stages. *ACS Nano* **2013**, *7*, 10158−10166.
(35) A Revolution for Laminar Flow. 2020. https://www.sulzer.com/en/shared/products/static-mixer-smx-plus.
(36) Yang, H.; Luan, W.; Tu, S. T.; Wang, Z. M. Synthesis of nanocrystals via microreaction with temperature gradient: towards separation of nucleation and growth. *Lab Chip* **2008**, *8*, 451−5.
(37) Tessier, M. D.; De Nolf, K.; Dupont, D.; Sinnaeve, D.; De Roo, J.; Hens, Z. Aminophosphines: A Double Role in the Synthesis of Colloidal Indium Phosphide Quantum Dots. *J. Am. Chem. Soc.* **2016**, *138*, 5923−5929.
(38) Ramasamy, P.; Kim, B.; Lee, M. S.; Lee, J. S. Beneficial Effects of Water in the Colloidal Synthesis of InP/ZnS Core-Shell Quantum Dots for Optoelectronic Applications. *Nanoscale* **2016**, *8*, 17159−17168.
(39) Akiyama, Y.; Fujita, S.; Senboku, H.; Rayner, C. M.; Brough, S. A.; Arai, M. An in situ high pressure FTIR study on molecular interactions of ketones, esters, and amides with dense phase carbon dioxide. *J. Supercrit. Fluids* **2008**, *46*, 197−205.
(40) Max, J. J.; Chapados, C. Infrared spectroscopy of aqueous carboxylic acids: Comparison between different acids and their salts. *J. Phys. Chem. A* **2004**, *108*, 3324−3337.
(41) De Berti, I. O. P.; Cagnoli, M. V.; Pecchi, G.; Alessandrini, J. L.; Stewart, S. J.; Bengoa, J. F.; Marchetti, S. G. Alternative low-cost approach to the synthesis of magnetic iron oxide nanoparticles by thermal decomposition of organic precursors. *Nanotechnology* **2013**, *24*, 1−11.

https://dx.doi.org/10.1021/acsanm.0c02814
ACS Appl. Nano Mater. 2020, 3, 12325−12333

(42) Mourdikoudis, S.; Liz-Marzan, L. M. Oleylamine in Nanoparticle Synthesis. *Chem. Mater.* **2013**, *25*, 1465−1476.
(43) Zhang, Z. H.; Lu, M. H.; Xu, H. R.; Chin, W. S. Shape-controlled synthesis of zinc oxide: A simple method for the preparation of metal oxide nanocrystals in non-aqueous medium. *Chem. - Eur. J.* **2007**, *13*, 632−638.
(44) Baquero, E. A.; Virieux, H.; Swain, R. A.; Gillet, A.; Cros-Gagneux, A.; Coppel, Y.; Chaudret, B.; Nayral, C.; Delpech, F. Synthesis of Oxide-Free InP Quantum Dots: Surface Control and H-2-Assisted Growth. *Chem. Mater.* **2017**, *29*, 9623−9627.
(45) Cros-Gagneux, A.; Delpech, F.; Nayral, C.; Cornejo, A.; Coppel, Y.; Chaudret, B. Surface chemistry of InP quantum dots: a comprehensive study. *J. Am. Chem. Soc.* **2010**, *132*, 18147−57.
(46) Zhang, Z. H.; Liu, S. H.; Chow, S. Y.; Han, M. Y. Modulation of the Morphology of ZnO Nanostructures via Aminolytic Reaction: From Nanorods to Nanosquamas. *Langmuir* **2006**, *22*, 6335−6340.
(47) Protière, M.; Reiss, P. Amine-induced growth of an In2O3 shell on colloidal InP nanocrystals. *Chem. Commun.* **2007**, *23*, 2417−2419.

https://dx.doi.org/10.1021/acsanm.0c02814
ACS Appl. Nano Mater. 2020, 3, 12325−12333